

Article

Enhanced Visible Light Photocatalytic Degradation of Methylene Blue by CdS-ZnS-BiPO₄ Nanocomposites Prepared by a Solvent-Assisted Heating Method

Hsin-Chan Tsai ¹, Yu-Hui Peng ¹, Po-Yu Wen ¹, Tsunghsueh Wu ^{2,*} and Yang-Wei Lin ^{1,*}

¹ Department of Chemistry, National Changhua University of Education, 1, Jin-De Road, Changhua City 5007, Taiwan; sinzent123@yahoo.com.tw (H.-C.T.); a8428625625@gmail.com (Y.-H.P.); bba02123@gmail.com (P.-Y.W.)

² Department of Chemistry, University of Wisconsin-Platteville, 1 University Plaza, Platteville, WI 53818-3099, USA

* Correspondence: wut@uwplatt.edu (T.W.); linywjerry@cc.ncue.edu.tw (Y.-W.L.); Tel.: +1-608-342-6018 (T.W.); +886-4-7232105-3553 (Y.-W.L.)

Citation: Tsai, H.-C.; Peng, Y.-H.; Wen, P.-Y.; Wu, T.; Lin, Y.-W. Enhanced Visible Light Photocatalytic Degradation of Methylene Blue by CdS-ZnS-BiPO₄ Nanocomposites Prepared by a Solvent-Assisted Heating Method. *Catalysts* **2021**, *11*, 1095. <https://doi.org/10.3390/catal11091095>

Academic Editor: Danilo Russo

Received: 12 August 2021

Accepted: 9 September 2021

Published: 11 September 2021

Publisher's Note: MDPI stays neutral with regard to jurisdictional claims in published maps and institutional affiliations.



Copyright: © 2021 by the authors. Licensee MDPI, Basel, Switzerland. This article is an open access article distributed under the terms and conditions of the Creative Commons Attribution (CC BY) license (<http://creativecommons.org/licenses/by/4.0/>).

Abstract: In this study, a ternary CdS-ZnS-BiPO₄ nanocomposite, synthesized by a solvent-assisted heating method, demonstrated the highest visible light-induced photocatalysis towards the degradation of methylene blue (MB) when comparing with BiPO₄, CdS-BiPO₄, and ZnS-BiPO₄. Transmission electron microscopy (TEM), X-ray powder diffraction (XRD), and UV-Vis diffuse reflectance spectroscopy (UV-vis DRS) were used to characterize the prepared nanocomposites. From UV-DRS results, the energy band gap of the prepared BiPO₄ structures was 4.51 eV. When CdS nanoparticles were deposited on BiPO₄ surface by a solvent-assisted heating method, the prepared nanocomposites exhibited visible light-responsive photocatalytic degradation toward MB (20 ppm). At a molar ratio of Cd to Zn as 1:7, the prepared CdS-ZnS-BiPO₄ nanocomposites exhibited the best photocatalytic activity in degrading 95% of MB dyes, out-performing pure BiPO₄, CdS-BiPO₄, and ZnS-BiPO₄ due to its enhanced charge separation efficiency and the lowered carrier recombination from the efficient p-n junction of unprecedented ternary composites. The investigations on mechanism conclude that the major reactive species responsible for MB degradation are holes and oxygen radicals. For practicality, the degradation efficiency for different dyestuff (Fast Green FCF, Rhodamine 6G, Acid Blue 1, methyl orange, and methyl red) degradation in the different water matrix samples (pond water, seawater, and lake water) by the prepared CdS-ZnS-BiPO₄ nanocomposites was evaluated.

Keywords: solvent-assisted heating; CdS-ZnS-BiPO₄; white-light LED; photocatalytic degradation

1. Introduction

Apparel plays an important role in our society and contributes to a large part of the global economy; however, the typical textile dyeing method involves excess amounts of dyestuffs, which are eventually discharged as wastewater, imposing technical challenges on the wastewater treatment facility [1–3]. Adsorption, filtration, coagulation, and biodegradation are all traditional processes used in the water treatment industry [4–9]. These approaches have limitations in terms of cost, feasibility, time required, and environmental impacts [10]. Despite the fact that adsorption is a common process for removing toxic textile dyes it could be incapable of degrading or mineralizing organic contaminants from the environment [11]. To make matter worse, some dyes are relatively stable such that conventional water treatments are limited in the decolorization of dyes. Among the different methods, photodegradation using semiconductor metal oxide is a potential green environmental protection technique because it can directly break down dye molecules in

effluent to harmless ones, such as CO₂ and H₂O. Thus, a new method of employing photocatalysts in breaking down dyes has been developed as an alternative option for effective treatment of wastewater containing organic dyes [12–18]. In the pioneer work, TiO₂ catalyst was attractive due to its nontoxicity, low cost, and high chemical stability [19]. However, with low quantum efficiency (<20%), the photocatalytic activity of TiO₂ is inefficient, leading to high operation cost for industrial applications as high-energy UV light is required for water treatment [20]. Its shortcoming arises from its high charge recombination rate in its inherited material property. As a result, research efforts in improving photocatalytic materials have been made to meet the current challenge in the textile industry [2].

Some novel materials, such as BiPO₄ photocatalysts, were synthesized in 2014 to find materials with high photocatalytic activity [21,22]. The high charge separation efficiency made BiPO₄ photocatalysts highly photocatalytic. However, its poor visible light responsiveness limits its applicability in degrading the dyestuffs. Many systematic follow-up works have analyzed the morphology-dependent photocatalytic performance and found ways to improve the visible light absorption characteristics which enable sunlight-induced catalysis, a promising technology for future sustainable wastewater treatment options [23]. In 2012, the BiPO₄–CdS composites with varying CdS compositions were prepared using a microwave-assisted method, and their performance in the degradation of 10 ppm methyl orange (MO) under visible light irradiation was evaluated [24]. The results show that the BiPO₄–CdS composite (30.1 wt% CdS) performed the best as 98.1% of MO degraded by a 400 W halogen lamp (>400 nm) within 5 h due to the enhanced visible light absorption. However, cadmium is a toxic constituent in the photocatalyst developed from cadmium chloride, potentially imposing environmental issues during the synthesis and water treatment [25,26]. To dilute the concentration of toxic cadmium-ions as an alternate photocatalyst option, PVP-capped ZnS (20 wt%) and CdS nanoparticle mixtures were synthesized using a microwave irradiation method and demonstrated good visible light-induced degradation of 10 ppm methylene blue (MB) solution and achieved 81% degradation after 6 h of halogen lamp irradiation (500 W, emission range of 400–800 nm, without filter) [27]. Therefore, we expected the photocatalytic activity of BiPO₄–CdS composite to be improved by mixing with ZnS nanoparticles due to its sufficient negative conduction band bottom potential for the photodegradation process [28,29]. To investigate the optimal composition of photocatalysts, a series of experiments was carried out on CdS–ZnS–BiPO₄ nanocomposites with different molar ratios of Cd/Zn precursor. In addition, there has been no report on the proposed one-pot synthetic approach for a ternary nanomaterial and investigation of CdS–ZnS–BiPO₄ nanocomposites for photocatalysis until now.

In this study, we provided four interesting results about XS–BiPO₄ nanocomposites (X = Cd, Zn). First, a solvent-assisted heating synthesis of CdS–BiPO₄, ZnS–BiPO₄ and CdS–ZnS–BiPO₄ nanocomposites was demonstrated. Ethylene glycol was used as a solvent to allow high-temperature heating of reactants enabling the formation of intimate contact between the components as a crucial requirement for outstanding interfacial properties such as electronic interaction and charge transfer. Second, another goal of this study is to use a light emitting diode (LED) (400–800 nm, 0.42 W/cm²) as a light source for light irradiation. Third, the photocatalytic activity and practicability of the prepared nanocomposites were evaluated from its ability to degrade MB, Fast Green FCF (FCF), rhodamine 6G (R6G), Acid Blue 1 (SB), MO, and methyl red (MR) in different water matrix samples under visible light irradiation. Finally, the possible photocatalytic mechanism for the MB degradation of the prepared XS–BiPO₄ nanocomposites (X = Cd, Zn) was elucidated through scavenging experiments.

2. Results and Discussion

2.1. Characterization of CdS-BiPO₄, ZnS-BiPO₄, and CdS-ZnS-BiPO₄

Figure 1A displays the morphologies and composition of BiPO₄, CdS-BiPO₄, ZnS-BiPO₄ and CdS-ZnS-BiPO₄ nanocomposites analyzed by TEM and energy dispersive spectrometer (EDS). First, the BiPO₄ sample prepared by the hydrothermal method appears rod-shaped and measures 1–2 μm in length and 150 nm in width. EDS analysis also reveals 60.68% (wt%) Bi, 8.02% P, and 31.3% O elements in the BiPO₄ sample. TEM image of CdS-BiPO₄ nanocomposites shows CdS nanoparticles with size of 5 ± 3 nm were deposited on the BiPO₄ surface. EDS analysis reveals 63.9% Bi, 10.25% P, 24.31% O, 1.13% Cd, and 0.41% S elements in CdS-BiPO₄ nanocomposites. For ZnS-BiPO₄ nanocomposites, ZnS nanoparticles were deposited on the surface of BiPO₄ and 66.3% Bi, 7.92% P, 23.52% O, 1.38% Zn, and 0.88% S elements are present in the ZnS-BiPO₄ nanocomposites from EDS analysis. As materials used for control experiments, CdS, ZnS, and CdS-ZnS nanoparticles were prepared and analyzed by TEM and HR-TEM as shown in Figure 1B. Some CdS-ZnS nanoparticles were found in TEM and HR-TEM images as core-shell particles, which are shown in Figure 1B. Finally, for CdS-ZnS-BiPO₄ nanocomposites (the precursor solution containing the molar ratio of Cd to Zn at 1:7), CdS-ZnS nanoparticles deposited on the BiPO₄ surface during EDS analysis confirms the presence of 60.48% Bi, 8.91% P, 26.53% O, 2.2% Zn, 0.29% Cd, and 1.29% S elements.

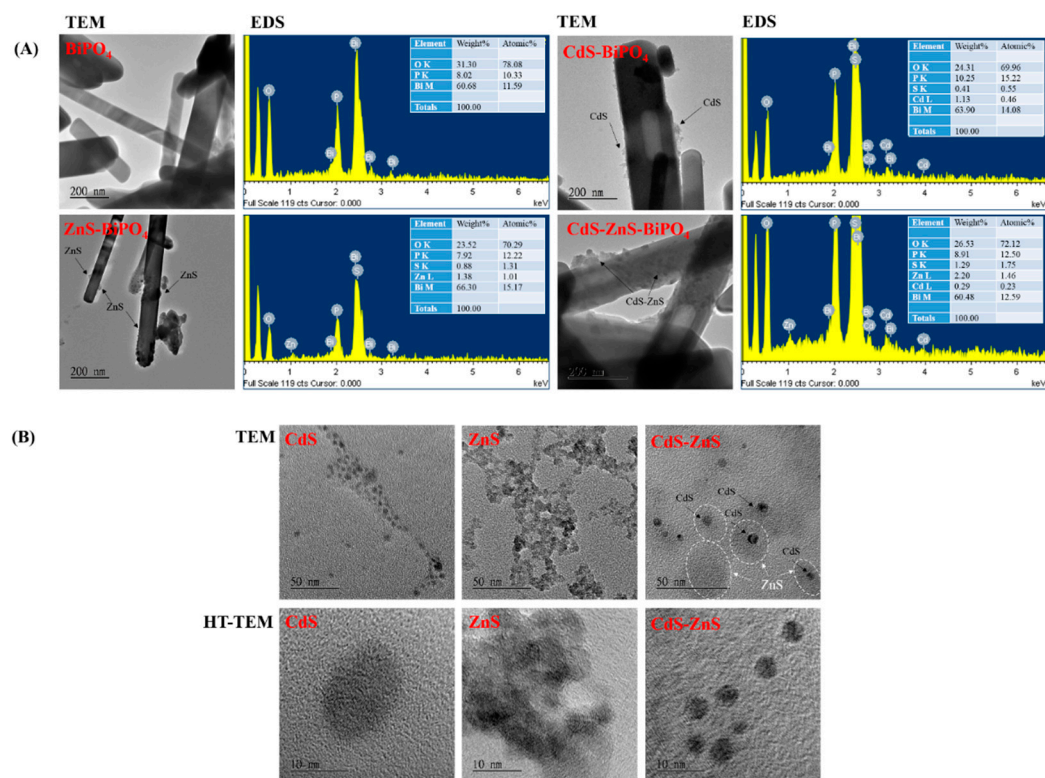


Figure 1. (A) TEM images and EDS spectra of BiPO₄, CdS-BiPO₄, ZnS-BiPO₄, and CdS-ZnS-BiPO₄ (the precursor solution contained the molar ratio of Cd to Zn at 1:7) nanocomposites. (B) TEM and HR-TEM images of CdS, ZnS, and CdS-ZnS (the precursor solution contained the molar ratio of Cd to Zn at 1:7) nanoparticles.

The phases and purities of the products were identified via XRD analysis. The XRD pattern of BiPO₄ as shown in Figure 2 was in agreement with the standard data of pure monoclinic BiPO₄ (JCPDS 80-0209) [23]. For CdS-BiPO₄, ZnS-BiPO₄, and CdS-ZnS-BiPO₄ nanocomposites, the XRD patterns of these samples were similar to that of BiPO₄. The main peaks for hexagonal CdS nanoparticles (JCPDS 77-2306, 2θ values at 24.8°, 26.5°, 28.2°, 36.6°, 43.7°, and 51.8°) and cubic ZnS nanoparticles (JCPDS 65-0309, 2θ values at

28.6°, 47.6°, and 56.5°) as shown in enlarge spectra of Figure 2 were not found in CdS-BiPO₄, ZnS-BiPO₄, and CdS-ZnS-BiPO₄ nanocomposites [27]. This may be because only a few CdS, ZnS, and CdS-ZnS nanoparticles were deposited onto the BiPO₄ surface, and the signal was overwhelmed by the presence of BiPO₄.

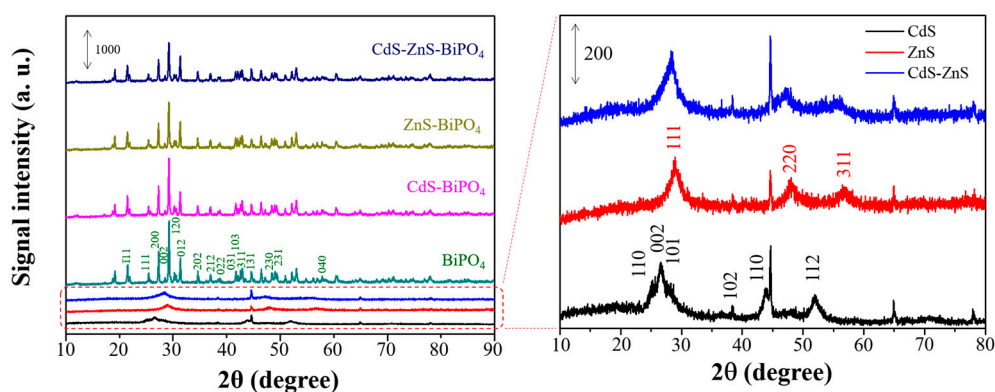


Figure 2. XRD spectra of CdS-BiPO₄, ZnS-BiPO₄, CdS-ZnS-BiPO₄, CdS, ZnS, and CdS-ZnS samples.

To determine the bandgap, the UV–vis DRS spectra shown in Figure 3 were analyzed. BiPO₄ sample displays a strong UV light absorption from 200 nm to 275 nm wavelength but a very weak absorption after 275 nm, indicating a weak absorption of near-UV and visible-light; thus, this material is not suitable to be used as a sunlight-responsive photocatalyst. After depositing CdS onto BiPO₄, the absorption in visible light was significantly improved up to 550 nm in CdS-BiPO₄ composites. Incorporating ZnS into BiPO₄ only exhibits UV light absorption, indicating that ZnS-BiPO₄ nanocomposites can absorb UV absorption like BiPO₄ samples. Similar to CdS-BiPO₄ nanocomposites, CdS-ZnS-BiPO₄ nanocomposites exhibit strong absorption in UV and visible regions from 200 nm to 500 nm even though the precursor for zinc ions is seven times higher than cadmium ions in synthesis. The comparison between the absorption characteristics of the BiPO₄ composites in Figure 3A and the absorption characteristics of nanoparticles without BiPO₄ in Figure 3C strongly confirms that the visible light absorption for CdS-BiPO₄, ZnS-BiPO₄, and CdS-ZnS-BiPO₄ nanocomposites was entirely attributed to hybrid CdS, ZnS, and CdS-ZnS nanoparticles.

The band gap energy (E_g) can be evaluated from the UV-DRS spectra via a $Tauc$ plot of $(h\nu)^{0.5}$ versus $(h\nu)$ and extrapolation of the linear portions of the curves to the energy axis as shown in Figures 3B,D:

$$\alpha h\nu = B(h\nu - E_g)^2$$

where α is the absorption coefficient, $h\nu$ is the photo energy, E_g is the indirect band gap energy, and B is a constant. The estimated optical band gaps of the prepared samples are shown in Table 1. The band gap value of BiPO₄ is 4.03 eV corresponding to UV region absorption. The band gap values for CdS and ZnS nanoparticles are 2.75 eV and 3.98 eV, respectively and higher than their bulk counterparts, which is due to reduced particle size showing quantum confinement effects [27]. The band gap value of CdS-ZnS nanoparticles is 3.08 eV and is located between that of CdS and ZnS nanoparticles. The band gap values of CdS-BiPO₄, ZnS-BiPO₄, and CdS-ZnS-BiPO₄ nanocomposites are 2.27 eV, 3.01 eV, and 2.43 eV, respectively. These results clearly confirm that the electronic structures of all nanocomposites differ from BiPO₄. The variation in the bandgap may be due to depositing different types of nanoparticles, resulting in different degrees of charge separation efficiency and recombination rates of the photoinduced electron–hole pairs. This caused the prepared nanocomposites to have different photocatalytic efficiencies.

Table 1. Measured energy gap (E_g), the level of conduction-band (CB) edge, and valence-band edge (VB) for the prepared samples.

Series	E_g (eV)	CB (V)	VB (V)
CdS	2.75	-1.00	1.75
ZnS	3.98	-1.43	2.55
CdS-ZnS	3.08	- ^a	- ^a
BiPO ₄	4.03	0.41	4.51
CdS-BiPO ₄	2.27	- ^a	- ^a
ZnS-BiPO ₄	3.01	- ^a	- ^a
CdS-ZnS-BiPO ₄	2.48	- ^a	- ^a

^a When p-type CdS, ZnS, or CdS-ZnS come into contact with n-type BiPO₄ to form a p-n junction, the Fermi energy levels of CdS, ZnS, CdS-ZnS, and BiPO₄ tend to ascend and descend to achieve an equilibrium state, and it was difficult to calculate the VB edge and CB edge potential for the prepared nanocomposites. Because of no $\chi_{\text{CdS-ZnS}}$ value, there is no VB edge and CB edge potential for CdS-ZnS nanoparticles.

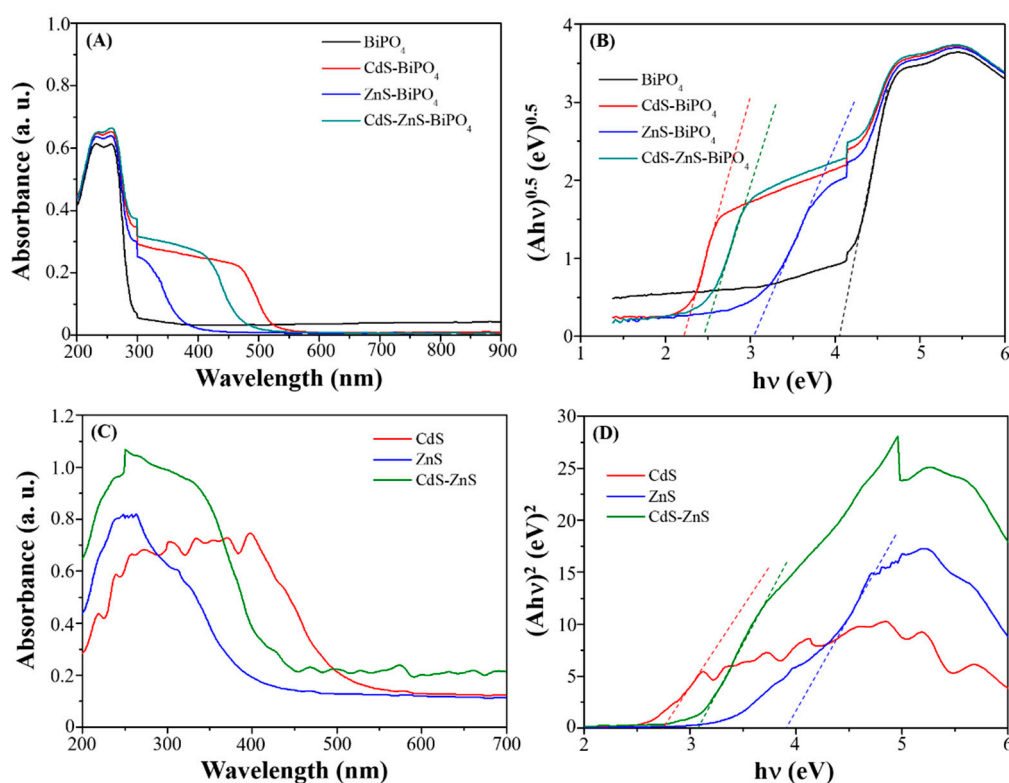


Figure 3. (A) UV-vis DRS spectra and (B) $(A)h\nu)^{0.5}$ versus $h\nu$ curves of BiPO₄ (black), CdS-BiPO₄ (red), ZnS-BiPO₄ (blue), and CdS-ZnS-BiPO₄ (olive) composites. (C) UV-vis DRS spectra and (D) $(A)h\nu)^2$ versus $h\nu$ curves of CdS (red), ZnS (blue), and CdS-ZnS (olive) nanoparticles.

2.2. Degradation Performance of BiPO₄, CdS-BiPO₄, ZnS-BiPO₄, and CdS-ZnS-BiPO₄

The photocatalytic performance of BiPO₄, CdS-BiPO₄, ZnS-BiPO₄, and CdS-ZnS-BiPO₄ nanocomposites was evaluated by measuring the rate of MB degradation (20 ppm) under visible irradiation. According to our previous experience, the degradation efficiency decreased with increasing dye concentration [23,30–34]. This is because the excessive coverage of dye on the active surface of photocatalysts leads to a decrease in the photocatalytic activity. Thus, 20 ppm MB was selected for the experiment. The variations in the MB concentration (C/C_0), where C_0 is the initial MB concentration, and C is the MB concentration at time t , with the irradiation time for BiPO₄, CdS-BiPO₄, ZnS-BiPO₄, and

CdS-ZnS-BiPO₄ nanocomposites were found in Figure 4A. Prior to irradiation, each catalyst (0.20 g) was introduced to the 20 ppm MB solution for 30 min (indicated as “–30 min” in Figure 4A) in the dark for the system to reach equilibrium. The change in MB concentration for each composite after this equilibration time is found negligible, reflecting negligible dye adsorption on each nanocomposite. As another control experiment, direct photolysis of MB without any photocatalysts was also analyzed under identical conditions, and no change was found in MB concentration during 60 min photolysis (Figure A2). In addition, the results of MB degradation in the presence of CdS, ZnS, and CdS-ZnS nanoparticles were also found in Figure A2. The degradation efficiency within 60 min irradiation time followed the order: CdS-ZnS (55%) > CdS (40%) > ZnS (10%), indicating that the CdS-ZnS nanoparticles had higher photocatalytic activity. The result was the same as the previous literature [27]. From Figure 4A, the MB variation changes only slightly after photolysis in the presence of BiPO₄ and ZnS-BiPO₄ nanocomposites due to weak absorption of visible light from its high-energy band gap discussed earlier. In contrast, the extent of MB degradation (87% degradation efficiency) changed dramatically within the 60 min of light irradiation in the presence of the CdS-BiPO₄ nanocomposites. Furthermore, the highest degradation efficiency (95% within 60 min) was found in the presence of CdS-ZnS-BiPO₄ nanocomposites due to the different degrees of charge separation efficiency and recombination rate, which will be discussed in the degradation mechanism section.

The photocatalytic degradation kinetics for MB was then investigated as shown in Figure 4B, and the photodegradation process matched with a pseudo first-order reaction model. The rate constants (*k*) for MB degradation by BiPO₄, CdS-BiPO₄, ZnS-BiPO₄, and CdS-ZnS-BiPO₄ nanocomposites were determined to be 0.0008, 0.0339, 0.0011, and 0.0461 min⁻¹, respectively. Clearly, the rate constant for CdS-ZnS-BiPO₄ is almost 57.6 times higher than that for BiPO₄. The relative kinetic parameters are summarized in Table 2. In addition, the degradation quantum yields of BiPO₄, CdS-BiPO₄, ZnS-BiPO₄, and CdS-ZnS-BiPO₄ are 0.0703, 2.98, 0.0966, and 4.05, respectively. These results designate the quantum yield of the CdS-ZnS-BiPO₄ nanocomposites is elevated when compare to the BiPO₄, ZnS-BiPO₄, and CdS-BiPO₄ photocatalyst.

Table 2. Pseudo-first-order rate constants for photocatalytic MB degradation by the prepared composites under visible light irradiation.

Series	Pseudo-First-Order Kinetic Equation	k (min ⁻¹)	R ²
BiPO ₄	y = 0.0008x – 0.0201	0.0008	0.9787
CdS-BiPO ₄	y = 0.0339x + 0.0043	0.0339	0.9891
ZnS-BiPO ₄	y = 0.0011x + 0.0178	0.0011	0.9512
CdS-ZnS-BiPO ₄	y = 0.0461 – 0.0998	0.0461	0.9851

To understand the role of Cd in the catalyst for the MB degradation, different molar ratios of Cd to Zn from the precursors used in the preparation of CdS-ZnS-BiPO₄ nanocomposites were evaluated as shown in Figure 5A. The photocatalytic activity increases initially as the Cd/Zn ratio decreases from 1:0 to 1:7 and the catalytic performance peaks at 1:7 Cd/Zn ratio. Then, further increase in Zn content from Cd/Zn 1:7 ratio decreased its photodegradation ability due to high content of ZnS nanoparticles in the CdS-ZnS-BiPO₄ nanocomposites decreasing the visible light absorption. Thus, the molar ratio of Cd to Zn was selected to be 1:7 in the preparation of CdS-ZnS-BiPO₄. The loading effect of CdS-ZnS-BiPO₄ nanocomposites on photodegradation of MB was evaluated and the results are shown in Figure 5B. During 60 min light irradiation, increasing mass of CdS-ZnS-BiPO₄ nanocomposites from 0.05 g to 0.20 g increased the degradation rate from 49.5% to 94.5%. Further increase in the mass of CdS-ZnS-BiPO₄ nanocomposites to 0.40 g did not increase the degradation rate. Thus, the optimum mass of CdS-ZnS-BiPO₄ was selected to be 0.2 g for further study.

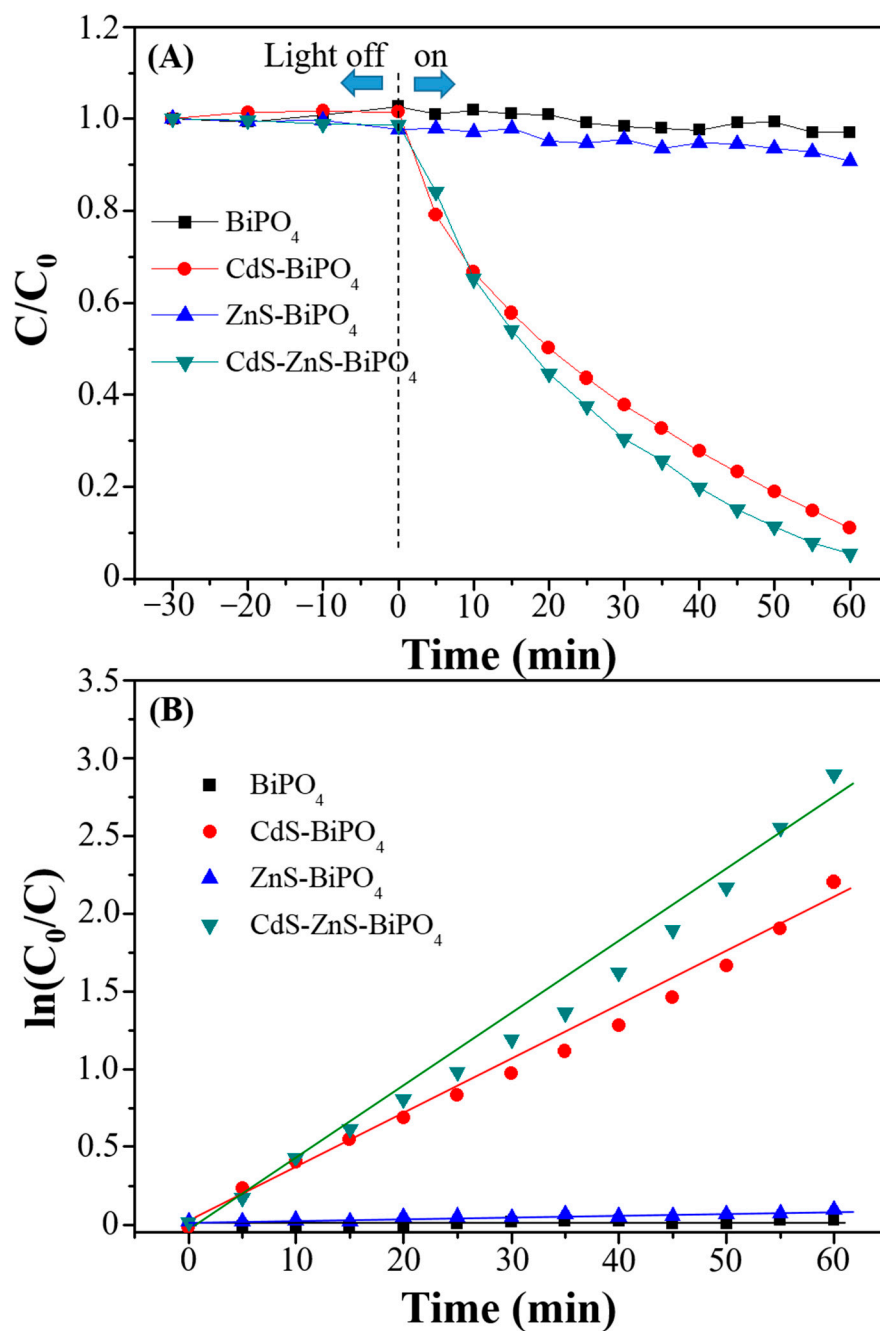


Figure 4. (A) Degradation of MB (C/C_0) over time and (B) the corresponding pseudo-first order linear transform of MB degradation rate in the presence of BiPO_4 (black), CdS-BiPO_4 (red), ZnS-BiPO_4 (blue), and CdS-ZnS-BiPO_4 (olive) nano-composites under visible light irradiation.

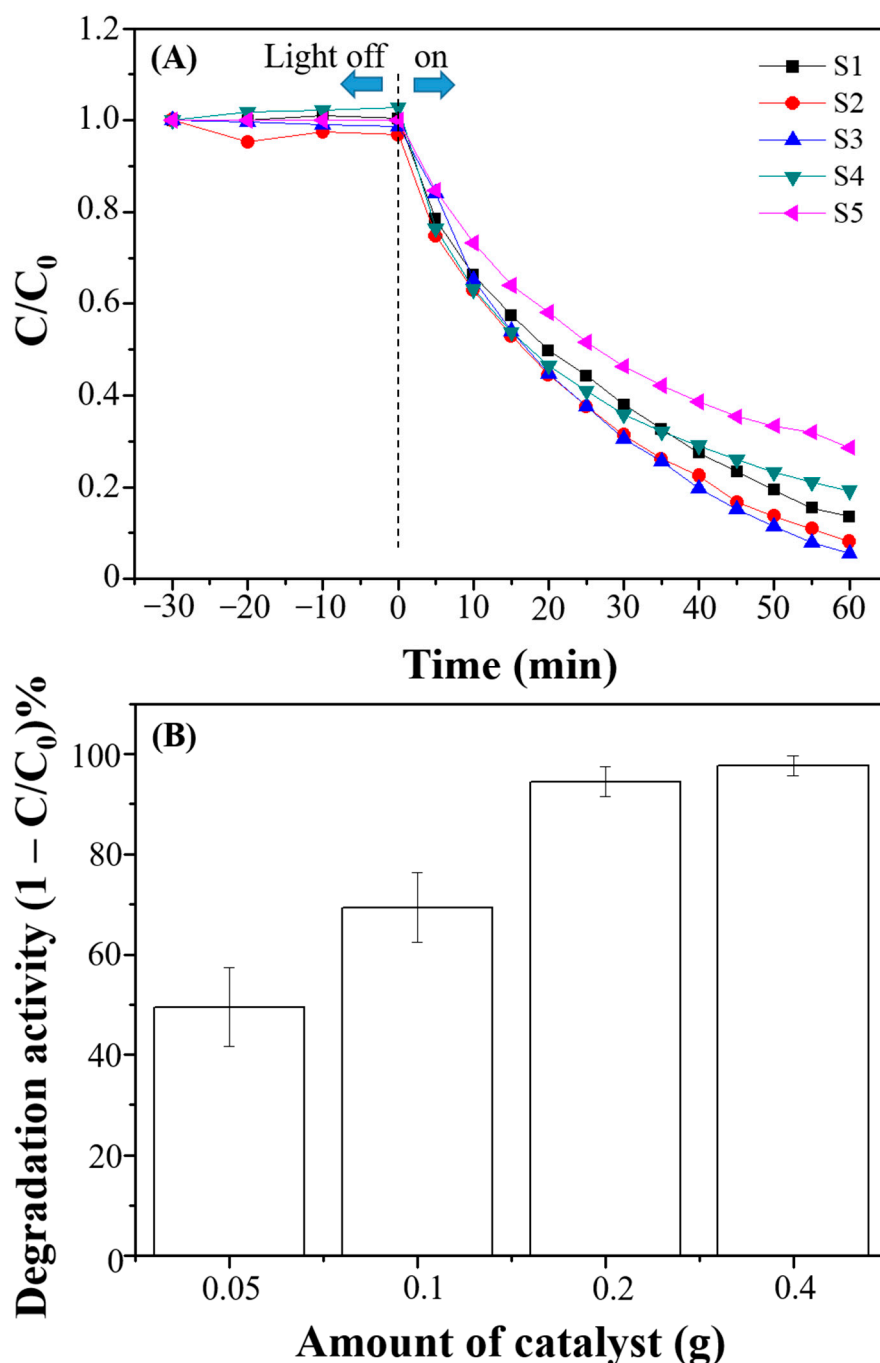


Figure 5. Degradation of MB (C/C_0) over time (A) in the presence of CdS-ZnS-BiPO₄ nanocomposites with different molar ratio of Cd to Zn, which 1:0, 1:5, 1:7, 1:9, and 1:11 are represented as S1, S2, S3, S4, and S5, respectively, and (B) degradation activity at different amounts of CdS-ZnS-BiPO₄ nanocomposites (Cd:Zn = 1:7) within 60 min light irradiation.

2.3. Degradation Mechanism of BiPO₄, CdS-BiPO₄, ZnS-BiPO₄, and CdS-ZnS-BiPO₄

In order to prove high-charge separation efficiency and low recombination rate of the photogenerated e^-/h^+ pairs made CdS-ZnS-BiPO₄ nanocomposites highly photocatalytic active, conventional instrumental methods, including electric impedance spectra (EIS), photocurrent and photoluminescence (PL) experiments were performed. First, the characteristics of charge separation were studied using EIS analysis. A high photocatalytic activity of a material often leads to a high charge separation efficiency, resulting in a low

charge resistance. Figure 6A summarizes *Nyquist* plots collected from nanocomposites. The diameter of semi-circles for the CdS-ZnS-BiPO₄ nanocomposites is the smallest when comparing to those of the BiPO₄, CdS-BiPO₄ and ZnS-BiPO₄ nanocomposites, suggesting that CdS-ZnS-BiPO₄ has the most efficient charge separation among all nanocomposites. The second best-performing photocatalyst in this study was CdS-BiPO₄ nanocomposites while the poorest performance was observed from BiPO₄ nanocomposites. Secondly, the photocurrent responses of BiPO₄, CdS-BiPO₄, ZnS-BiPO₄, and CdS-ZnS-BiPO₄ nanocomposites were found to evaluate the charge separation efficiency. Photocurrent responses of different nanocomposites are summarized in Figure 6B, in which photocurrent responses of CdS-BiPO₄ and CdS-ZnS-BiPO₄ are higher than those of BiPO₄ and ZnS-BiPO₄, demonstrating improved charge separation as a result of the p-n junction formed between P-type and N-type semiconductors. A p-n junction can improve the charge separation through the Schottky barrier effect, which is similar to a previous study on electron transfer from a semiconductor to a metal [19]. This contributes to the interfacial charge transfer between the semiconductors, thus improving the photocatalytic activity.

Reducing the recombination rate of the photogenerated e⁻/h⁺ pairs effectively made a material increasing the photocatalytic activity. Exothermic recombination of e⁻/h⁺ pairs can be studied through the measurement of PL; a low recombination rate is thus expected to produce a low luminescence intensity. The e⁻/h⁺ pairs recombination during MB degradation by the prepared nanocomposites was determined by PL (excitation wavelength: 325 nm) as shown in Figure 6C. The lowest luminescence intensity of the CdS-ZnS-BiPO₄ nanocomposites was obtained when comparing to those of the BiPO₄, CdS-BiPO₄, and ZnS-BiPO₄ nanocomposites, suggesting that the e⁻/h⁺ pairs recombination was restricted due to a p-n junction between CdS-ZnS nanoparticles and BiPO₄. In summary, the excellent photocatalytic activity of the CdS-ZnS-BiPO₄ nanocomposite was derived from a higher charge separation efficiency and a lower recombination rate than BiPO₄ and ZnS-BiPO₄ nanocomposites.

Radical- and hole-trapping experiments were performed to elucidate the photocatalytic degradation process for the CdS-ZnS-BiPO₄ nanocomposites. The MB degradation rate was suppressed by adding the hole and the oxygen radical scavenger (Figure 7) such as ethylenediamine tetraacetate (EDTA) and benzoquinone (BQ), respectively, but the degradation rate was only slightly inhibited upon the addition of the hydroxyl radical scavenger (*tert*-butanol (t-BuOH)) under visible light irradiation. As a result, holes and oxygen radicals are the primary active species involved in the decomposition of the adsorbed MB on the nanocomposites.

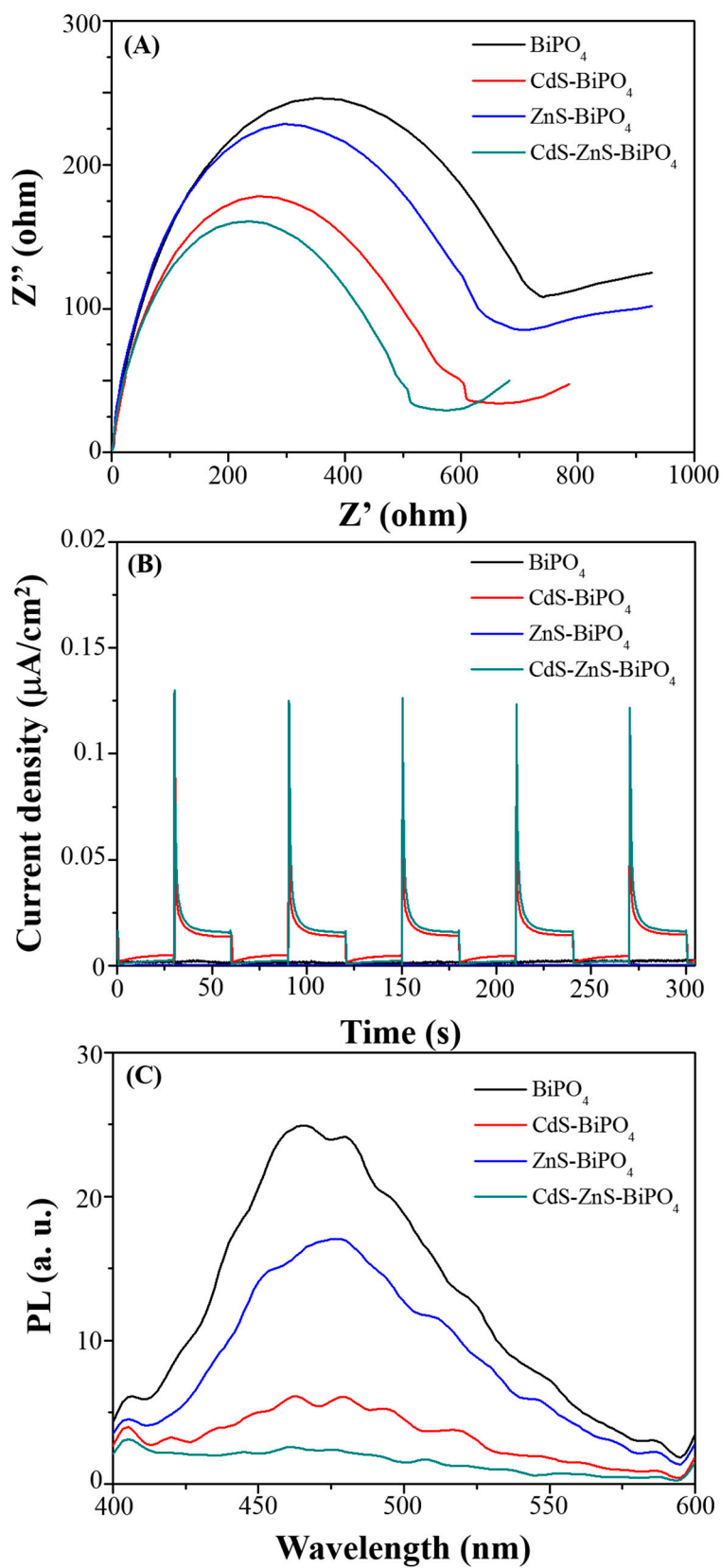


Figure 6. (A) EIS, (B) photocurrent, and (C) photoluminescence spectra of the BiPO₄ (black), CdS-BiPO₄ (red), ZnS-BiPO₄ (blue), and CdS-ZnS-BiPO₄ (olive) composites.

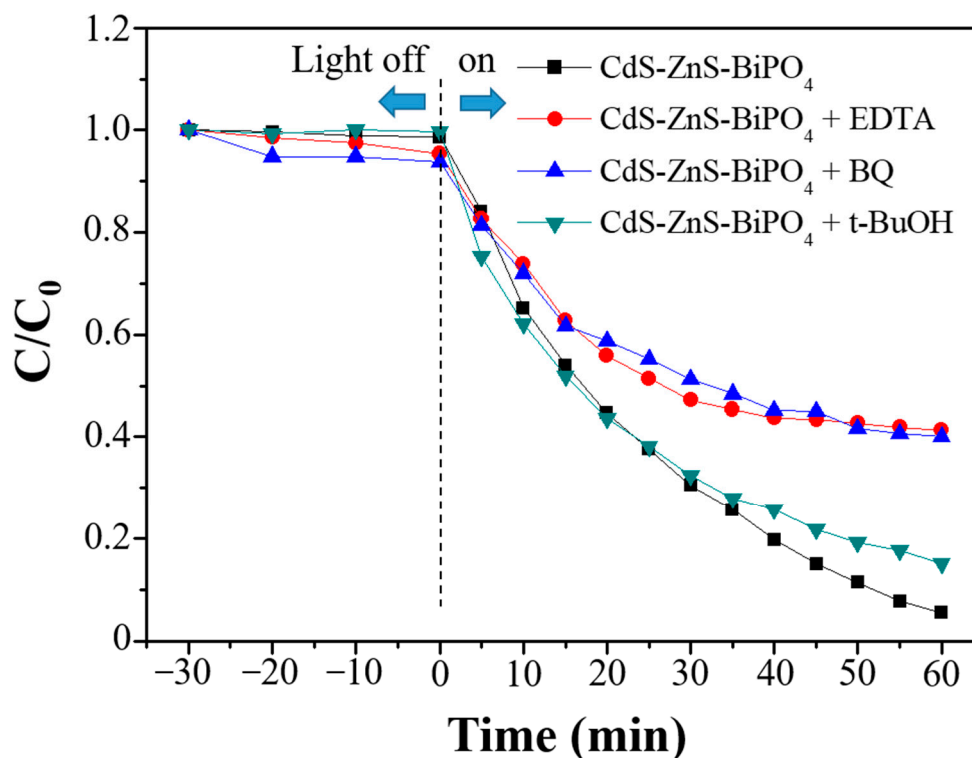


Figure 7. Trapping experiments of the CdS-ZnS-BiPO₄ nanocomposites for MB degradation (C/C_0) under visible light irradiation: EDTA, BQ, and t-BuOH (each 2 mM) were scavengers for holes, oxygen radicals, and hydroxyl radicals, respectively.

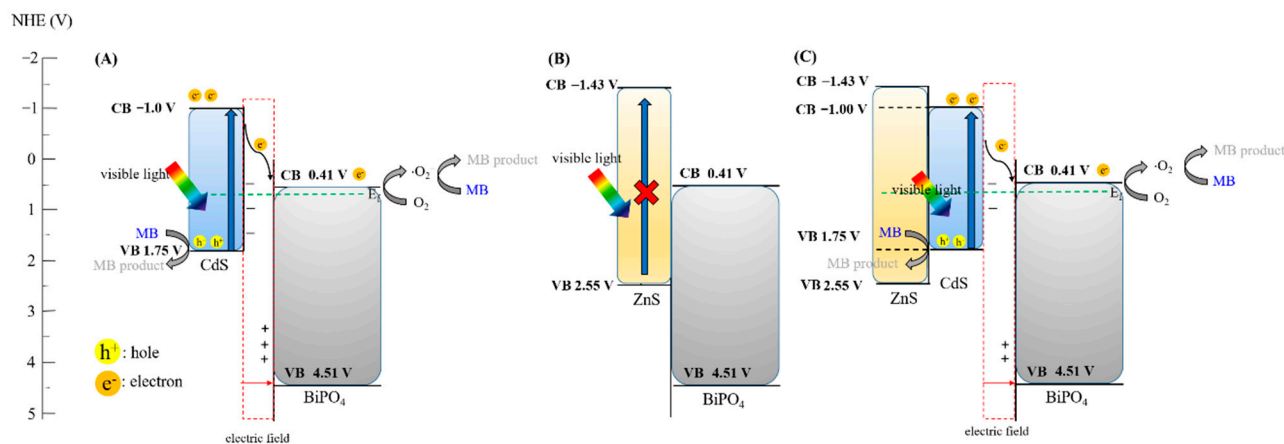
Based on the aforementioned studies, possible mechanisms for the prepared nanocomposites were proposed as shown in Scheme 1. The conduction band (CB) and valence band (VB) positions in BiPO₄, CdS, and ZnS nanoparticles as shown in Table 1 were calculated using the equation:

$$E_{VB} = X - E_c + 0.5E_g$$

$$E_{CB} = E_{VB} - E_g$$

where X is the Mulliken electronegativity (X_{BiPO_4} : 6.96 eV, X_{CdS} : 4.87 eV, X_{ZnS} : 5.06 eV), and E_c is the energy for free electrons of the hydrogen atom (≈ 4.5 eV). The photon energy of white-light LED can be efficiently absorbed by the CdS-BiPO₄ and CdS-ZnS-BiPO₄ nanocomposites, not by the ZnS-BiPO₄ nanocomposites. Considering the junction between CdS and BiPO₄, the electrons in the VB of the CdS nanoparticles can be excited to the CB and result in an equivalent number of holes. Because the CB of the CdS nanoparticles is higher than that of the BiPO₄ nanoparticles, partial electrons in CB of the CdS nanoparticles can migrate to the CB of the BiPO₄ nanoparticles. Thus, CdS-BiPO₄ nanocomposites form an efficient p-n junction interface. Once the electron reaches the CB of the BiPO₄ nanoparticles can react with oxygen to generate oxygen radicals; on the other hand, the accumulated holes on the CdS nanoparticles can oxidize organic substances (Scheme 1A). The junction between ZnS and BiPO₄ requires a larger energy gap than that of visible light provided. Thus, no p-n junction interface and no photocatalytic activity were found under white-light irradiation in the case of ZnS-BiPO₄ (Scheme 1B). For CdS-ZnS-BiPO₄, the electrons in the VB of the CdS nanoparticles can be excited to its CB with generation of the equivalent number of holes. Due to the larger energy gap and the VB and CB for ZnS nanoparti-

cles, the fate for the generated electrons in the CB of the CdS nanoparticles can only migrate to the CB of the BiPO₄ nanoparticles. Then, oxygen radicals produced at the CB of the BiPO₄ nanoparticles and the accumulated holes on the CdS nanoparticles were the major reactive species involving MB degradation (Scheme 1C). Compared to the CdS-BiPO₄ nanocomposites, ZnS nanoparticles provide a confinement effect for CdS nanoparticles; as a result, the only relaxation process for all excited electrons under visible light irradiation is to migrate to BiPO₄. Therefore, the CdS-ZnS-BiPO₄ nanoparticles have improved charge separation efficiency because of the confinement effect of the ZnS nanoparticles.



Scheme 1. Possible e⁻ movement in different degradation system of BiPO₄, CdS/BiPO₄, ZnS/BiPO₄, and CdS-ZnS-BiPO₄.

2.4. Practical Applications of CdS-ZnS-BiPO₄

For the practical applications of CdS-ZnS-BiPO₄, various organic dyes (FCF, R6G, SB, MO, and MR) were tested under visible light irradiation (Figure 8A). From the results, CdS-ZnS-BiPO₄ exhibited degradation activity toward all selected dyestuffs (nearly 54–95% degradation within 60 min). Finally, the prepared CdS-ZnS-BiPO₄ nanocomposites were used to degrade MB in the water matrix samples (Figure 8B) and found nearly 90% degradation efficiency on MB after 150 min of irradiation. The reduction of the photocatalytic performance of CdS-ZnS-BiPO₄ may be due to the presence of anions or radical scavengers in the water matrix samples. In addition, the seawater matrix leading to MB adsorption by CdS-ZnS-BiPO₄ was found, which may be due to the salting-out effect. Further work on the improvement of the photocatalytic performance with other heterojunction composites or under different light irradiation, such as carbon-based nanomaterials and II-VI group quantum dots, UV light, and LED monochromatic light source (420 nm, 450 nm, 485 nm, 535 nm, 595 nm, 630 nm), is underway in our laboratory.

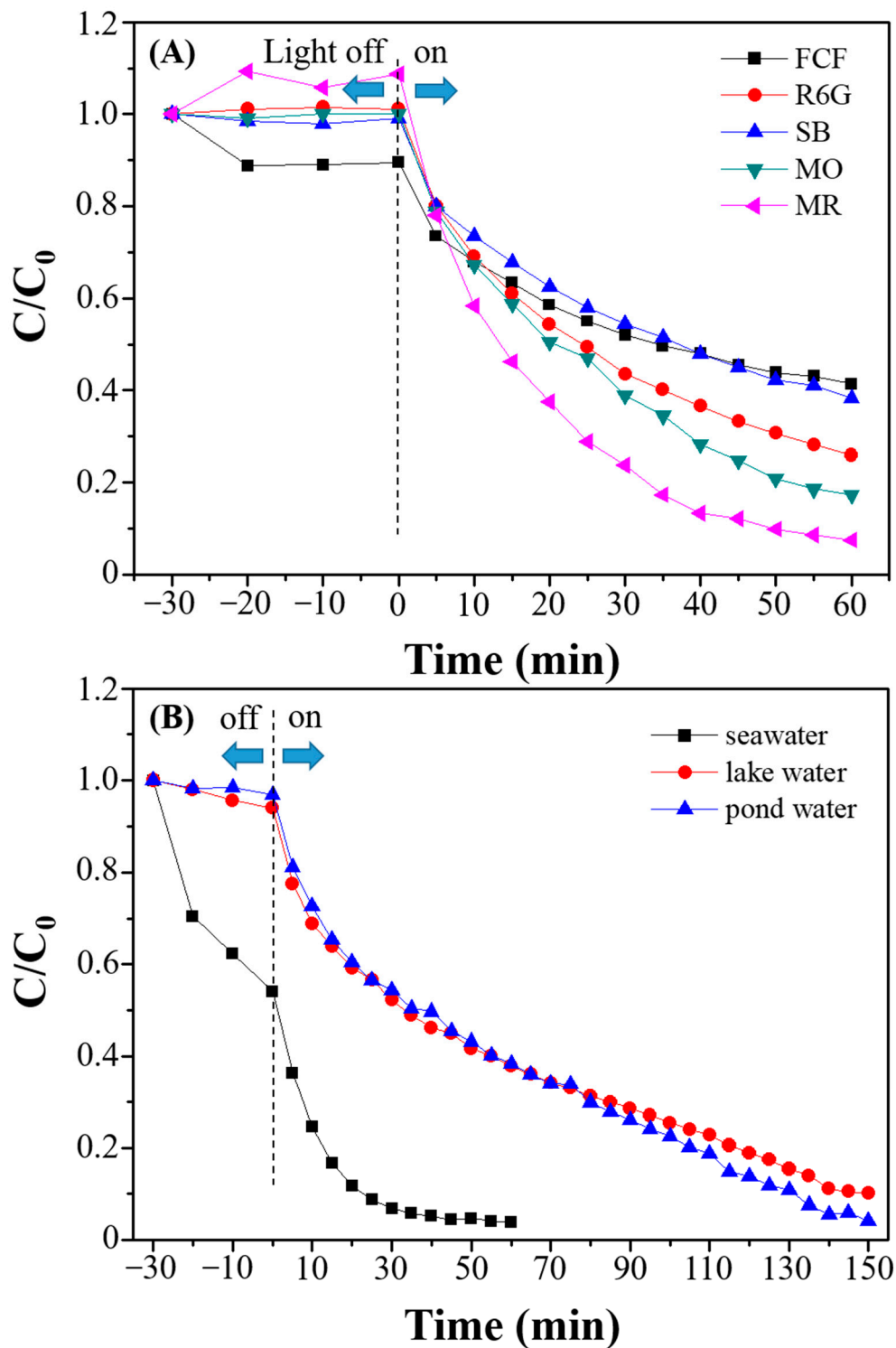


Figure 8. Photocatalytic degradation curves for (A) different dyestuff (FCF, R6G, SB, MO, and MR) and (B) MB in environmental water samples (seawater, pond water, and lake water) by CdS-ZnS-BiPO₄ nanocomposite.

3. Materials and Methods

3.1. Preparation of BiPO₄, CdS-BiPO₄, ZnS-BiPO₄, and CdS-ZnS-BiPO₄

All chemicals, including Bi(NO₃)₃·5H₂O, Na₃PO₄, Na₂S, ZnCl₂, CdCl₂, ethylene glycol (EG), poly(vinyl-pyrrolidone) (PVP, MW: 40000 g/mole), Na₂SO₄, ethanol, EDTA, t-BuOH, and BQ, were purchased from Sigma Aldrich (St. Louis, MO, USA). MB, Fast Green FCF, R6G, SB, MO, and MR were purchased from Invitrogen (Eugene, OR, USA). Milli-Q ultrapure water (18.3 MΩ) was used in all of the experiments.

For the preparation of BiPO₄ samples, HNO₃ (4 M, 1 mL) was used to dissolve Bi(NO₃)₃·5H₂O (0.6062 g) in a beaker. Then, ultrapure water (46 mL) and Na₃PO₄ (3 mL, 0.833 M) were added to the beaker, and the mixture was magnetically stirred at 27 °C. After 1 min, the mixture was delivered to a Teflon-lined stainless-steel autoclave and heated at 180 °C for 24 h. Finally, white BiPO₄ solids were separated by centrifugation. The solid was purified through a centrifuging-washing procedure (deionized water and ethanol, three times) and then dried in a desiccator at 60 °C overnight.

CdS-BiPO₄ nanocomposites were prepared through a solvent-assisted heating method. First, CdCl₂, Na₂S, and PVP precursor solutions were prepared by dissolving 1.500 g of CdCl₂, 3.9023 g of Na₂S, and 0.1255 g of PVP, respectively, in 50 mL of EG. The prepared BiPO₄ powder (0.3000 g) was dispersed in the CdCl₂ precursor solution (0.127 M, 8.182 mL) first with magnetic stirring at 170 °C to yield a uniform mixture. Then, EG (10 mL), Na₂S (0.517 M, 2.0 mL), and PVP (0.251%, 3.75 mL) were added to the above solution, and the mixture was magnetically stirred at 170 °C for 30 min. After the solution was naturally cooled to 27 °C, the precipitates were purified through a centrifuging-washing procedure (EG and ethanol, three times) and then dried at 60 °C overnight. For the preparation of ZnS-BiPO₄ nanocomposites, ZnCl₂ precursor solution (0.127 M, 8.182 mL) was used to replace CdCl₂ precursor solution, and the other procedure was the same as that mentioned above. In addition, similar procedure was performed to prepare CdS and ZnS nanoparticles without adding BiPO₄ powder.

The prepared BiPO₄ powder (0.3000 g) was dispersed in the Cd/Zn precursor solution (total volume: 8.182 mL), which was prepared by mixing 1.023 mL of CdCl₂ solution (0.127 M) and 7.159 mL of ZnCl₂ solution (0.127 M) first, with magnetic stirring at 170 °C to yield a uniform mixture. Then, EG (10 mL), Na₂S (0.517 M, 2.0 mL), and PVP (0.251%, 3.75 mL) were added to the above solution, and the mixture was magnetically stirred at 170 °C for 30 min. After the solution was naturally cooled to 27 °C, the precipitates were purified through a centrifuging-washing procedure (EG and ethanol, three times) and then dried at 60 °C overnight. For evaluation of the photocatalytic performance for CdS-ZnS-BiPO₄ nanocomposites with different molar ratios of Cd/Zn, different molar ratios of Cd/Zn precursor solutions were prepared as shown in Table 3. The rest of the procedure was the same as mentioned above.

Table 3. Preparation of different molar ratios of Cd/Zn precursor solutions.

Molar Ratio of Cd:Zn	Cd(NO ₃) ₂ (0.217 M)	ZnCl ₂ (0.217 M)
1:5	1.364 mL	6.818 mL
1:7	1.023 mL	7.159 mL
1:9	0.818 mL	7.364 mL
1:11	0.682 mL	7.500 mL

3.2. Characterization

The morphologies, the crystalline phases and the optical properties of the prepared nanocomposites were found by a JEOL-2010 transmission electron microscope (TEM) (JEOL Co., Ltd., Tokyo, Japan) at an accelerating voltage of 200 kV equipped with a QUANTAX Annular XFlash QUAD FQ5060 (Bruker Nano, Berlin, Germany), a SMART APEX II X-ray diffractometer (Bruker AXS, Billerica, MA, USA) with Cu Kα radiation (λ

= 0.15418 nm), and an Evolution 2000 UV–Vis spectrometer (Thermo Fisher Scientific Inc., Madison, WI, USA) with BaSO₄ employed as the reference, respectively.

3.3. Degradation Process

The prepared BiPO₄, CdS-BiPO₄, ZnS-BiPO₄, and CdS-ZnS-BiPO₄ nanocomposites were used to degrade MB under visible light irradiation in a PCX-50A multichannel photochemical reaction system equipped with an LED disc (400–800 nm, 0.42 W/cm², Beijing Perfectlight Technology Co., LTD., Beijing, China) (Figure A1) [35–37], and their photocatalytic activity was evaluated based on our earlier reports with modifications [23,30–34]. Prior to irradiation, 50 mL of 20 mg/L MB (20 ppm) aqueous solution containing 0.20 g of nanocomposites was stirred in the dark for 30 min. During illumination, 3.000 mL of suspension was taken by a pipette and centrifuged (10,000 rpm) to remove the nanocomposites. Then, MB content was determined colorimetrically at 665 nm using a Synergy H1 Hybrid Multi-Mode Microplate Reader (Biotek Instruments, Inc., Winooski, VT, USA) according to the Beer-Lambert law. The concentration of MB is proportional to absorbance of MB, so the degradation activity (efficiency) of MB can be calculated by

$$\text{Degradation activity} = \left(1 - \frac{A}{A_0}\right) \times 100\% = \left(1 - \frac{C}{C_0}\right) \times 100\%$$

where A₀, A, and C₀, C are the absorbance and concentration of MB when the irradiation time is 0 and t, respectively. Similar procedures were performed for various dyestuffs (FCF, R6G, SB, MO, and MR) and environmental water samples (seawater, pond water, and lake water). The reaction rate can be also calculated using plots of ln C₀/C versus irradiation time according to

$$\ln\left(\frac{C_0}{C}\right) = kt$$

where t is the irradiation time, and k is the pseudo-first-order rate constant of the reaction. The quantum yield of a photocatalytic reaction is defined as the number of MB molecules being degraded per photon absorbed. The rate constant of MB under visible light irradiation can also calculate its reaction quantum yield according to the following equation

$$\phi = \frac{k}{2.303I_0\epsilon_{\text{RF}}l}$$

where φ is the reaction quantum yield, k is the pseudo-first-order rate constant of the reaction, I₀ is the light intensity of the event light range at 400–800 nm (1.381 × 10⁻⁶), ε_{RF} is the molar absorptivity of MB at 420 nm (3.580 × 10³ cm⁻¹ M⁻¹), and l is the path length (1 cm) of the reaction [38].

3.4. Evaluation of Charge Separation and Recombination Rate

The charge separation efficiency and recombination rate for the prepared nanocomposites were evaluated based on our earlier reports [23,30–34]. For determination of recombination rate of e⁻/h⁺ pairs, PL spectra were collected using a Varian Cary Eclipse fluorescence spectrometer (Agilent Technologies, Inc., Santa Clara, CA, USA). An indium tin oxide (ITO) glass, coated by a slurry containing nanocomposite (5.0 mg) and methanol (5.0 mL), was heated on the hotplate at 50 °C for 30 min to completely evaporate the methanol. In the electrochemical cell, this coated ITO glass was used as an anode electrode, a platinum foil was used as a cathode electrode, and Na₂SO₄ solution (0.1 M) was used as a supporting electrolyte. Photocurrent tests and EIS, which was used to study the charge separation efficiency, were performed using a CHI-6122E electrochemical analyzer (CH instruments, Inc., Austin, TX, USA) at room temperature.

3.5. Free Radical Trapping Test

The free radical trapping test was used to obtain the major reactive species involved in the MB degradation. The procedure was similar to the degradation process except hole-, oxygen radical- and hydroxyl radical- scavengers (each 2 mM) were added to the MB solution prior to the addition of nanocomposite.

4. Conclusions

In this study, we have demonstrated a solvent-assisted heating method to prepare CdS-BiPO₄, ZnS-BiPO₄, and CdS-ZnS-BiPO₄ nanocomposites and evaluate their photocatalytic activities toward dyestuff degradation. The photocatalytic results indicate that (i) the CdS-ZnS-BiPO₄ nanocomposites possess better photocatalytic performances (95% within 60 min) than pure BiPO₄, CdS-BiPO₄, and ZnS-BiPO₄ nanocomposites under visible light irradiation; (ii) the photocatalytic performance of the CdS-ZnS-BiPO₄ nanocomposites is dependent on the molar ratio of Cd to Zn precursor solution, and the nanocomposite with molar ratio of Cd to Zn at 1:7 achieves the highest degradation efficiency; (iii) the enhancement of the photocatalytic performance is due to the improvement of charge separation efficiency and the reduction of recombination from the efficient p-n junction created in the CdS-ZnS-BiPO₄ composites; (iv) the photodegradation of MB and other dyestuff can be degraded with irradiation power density as low as 0.42 W/cm²; (v). This study proves that the strong photocatalytic activity of the CdS-ZnS-BiPO₄ nanocomposites possesses is promising for its applications toward photodegradation of organic pollutants in different water matrix samples.

Author Contributions: Conceptualization, H.-C.T. and Y.-W.L.; methodology, H.-C.T.; validation, Y.-W.L., T.W., and H.-C.T.; formal analysis, H.-C.T.; investigation, H.-C.T.; data curation, H.-C.T., Y.-H.P., and P.-Y.W.; writing—original draft preparation, Y.-W.L. and T.W.; writing—review and editing, Y.-W.L.; visualization, Y.-W.L.; supervision, Y.-W.L.; project administration, Y.-W.L.; funding acquisition, Y.-W.L. All authors have read and agreed to the published version of the manuscript.

Funding: This study was supported by the Ministry of Science and Technology of Taiwan under contract (MOST 110-2113-M-018-001).

Conflicts of Interest: The authors declare no conflict of interest.

Appendix A



Figure A1. The image of a multichannel photochemical reaction system. A detailed description of the multichannel photochemical reaction system can be found in the following link. <https://www.perfectlight.com.cn/Product/detail/id/35.html> (visited on 09/05/2021).

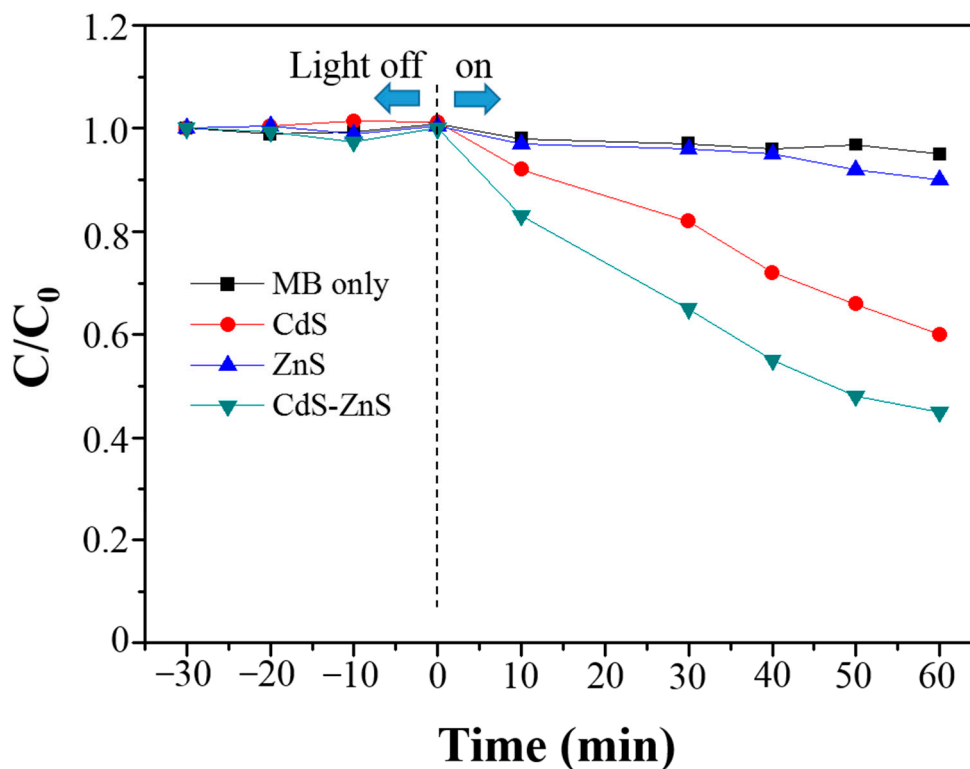


Figure A2. Degradation of MB (C/C_0) over time in the absence of catalyst (black), and the presence of CdS (red), ZnS (blue), and CdS-ZnS (olive) nanoparticles under visible light irradiation.

References

- Rafiq, A.; Ikram, M.; Ali, S.; Niaz, F.; Khan, M.; Khan, Q.; Maqbool, M. Photocatalytic Degradation of Dyes Using Semiconductor Photocatalysts to Clean Industrial Water Pollution. *J. Ind. Eng. Chem.* **2021**, *97*, 111–128.
- Behera, M.; Nayak, J.; Banerjee, S.; Chakraborty, S.; Tripathy, S.K. A Review on the Treatment of Textile Industry Waste Effluents Towards the Development of Efficient Mitigation Strategy: An Integrated System Design Approach. *J. Environ. Chem. Eng.* **2021**, *9*, 105277.
- Selvaraj, V.; Karthika, T.S.; Mansiya, C.; Alagar, M. An over Review on Recently Developed Techniques, Mechanisms and Intermediate Involved in the Advanced Azo Dye Degradation for Industrial Applications. *J. Mol. Struct.* **2021**, *1224*, 129195.
- Ben Mosbah, M.; Mechi, L.; Khiari, R.; Moussaoui, Y., Current State of Porous Carbon for Wastewater Treatment. *Processes* **2020**, *8*, 1651.
- Chowdhury, M.F.; Khandaker, S.; Sarker, F.; Islam, A.; Rahman, M.T.; Awual, M.R. Current Treatment Technologies and Mechanisms for Removal of Indigo Carmine Dyes from Wastewater: A Review. *J. Mol. Liq.* **2020**, *318*, 114061.
- Priyadarshini, M.; Das, I.; Ghangrekar, M.M. Application of Metal Organic Framework in Wastewater Treatment and Detection of Pollutants: Review. *J. Indian. Chem. Soc.* **2020**, *97*, 507–512.
- Samsami, S.; Mohamadi, M.; Sarrafzadeh, M.H.; Rene, E.R.; Firoozbahr, M. Recent Advances in the Treatment of Dye-Containing Wastewater from Textile Industries: Overview and Perspectives. *Process. Saf. Environ. Prot.* **2020**, *143*, 138–163.
- Liu, Q.M.; Zhou, Y.; Lu, J.; Zhou, Y.B. Novel Cyclodextrin-Based Adsorbents for Removing Pollutants from Wastewater: A Critical Review. *Chemosphere* **2020**, *241*, 125043.
- Yunus, Z.M.; Yashni, G.; Al-Gheethi, A.; Othman, N.; Hamdan, R.; Ruslan, N.N. Advanced Methods for Activated Carbon from Agriculture Wastes; a Comprehensive Review. *Int. J. Environ. Anal. Chem.* **2020**, doi:10.1080/03067319.2020.1717477.
- Mashuri, S.I.S.; Ibrahim, M.L.; Kasim, M.F.; Mastuli, M.S.; Rashid, U.; Abdullah, A.H.; Islam, A.; Mijan, N.A.; Tan, Y.H.; Mansir, N.; et al. Photocatalysis for Organic Wastewater Treatment: From the Basis to Current Challenges for Society. *Catalysts* **2020**, *10*, 1260.
- Deng, D.Y.; Lamssali, M.; Aryal, N.; Ofori-Boadu, A.; Jha, M.K.; Samuel, R.E. Textiles Wastewater Treatment Technology: A Review. *Water. Environ. Res.* **2020**, *92*, 1805–1810.

12. Giwa, A.; Yusuf, A.; Balogun, H.A.; Sambudi, N.S.; Bilad, M.R.; Adeyemi, I.; Chakraborty, S.; Curcio, S. Recent Advances in Advanced Oxidation Processes for Removal of Contaminants from Water: A Comprehensive Review. *Process. Saf. Environ. Prot.* **2021**, *146*, 220–256.
13. Din, M.I.; Khalid, R.; Najeeb, J.; Hussain, Z. Fundamentals and Photocatalysis of Methylene Blue Dye Using Various Nanocatalytic Assemblies- a Critical Review. *J. Clean. Prod.* **2021**, *298*, 126567.
14. Younis, S.A.; Maitlo, H.A.; Lee, J.; Kim, K.H. Nanotechnology-Based Sorption and Membrane Technologies for the Treatment of Petroleum-Based Pollutants in Natural Ecosystems and Wastewater Streams. *Adv. Colloid. Interf. Sci.* **2020**, *275*, 102071.
15. Tara, N.; Siddiqui, S.I.; Rathi, G.; Chaudhry, S.A.; Inamuddin; Asiri, A.M. Nano-Engineered Adsorbent for the Removal of Dyes from Water: A Review. *Curr. Anal. Chem.* **2020**, *16*, 14–40.
16. Bodzek, M.; Konieczny, K.; Kwiecinska-Mydlak, A. The Application of Nanomaterial Adsorbents for the Removal of Impurities from Water and Wastewaters: A Review. *Desalin. Water. Treat.* **2020**, *185*, 1–26.
17. Chenab, K.K.; Sohrabi, B.; Jafari, A.; Ramakrishna, S. Water Treatment: Functional Nanomaterials and Applications from Adsorption to Photodegradation. *Mater. Today. Chem.* **2020**, *16*, 100262.
18. Cheriyaundath, S.; Vavilala, S.L. Nanotechnology-Based Wastewater Treatment. *Water Environ. J.* **2021**, *35*, 123–132.
19. Hussain, S.M.; Hussain, T.; Faryad, M.; Ali, Q.; Ali, S.; Rizwan, M.; Hussain, A.I.; Ray, M.B.; Chatha, S.A.S. Emerging Aspects of Photo-Catalysts (TiO₂ & ZnO) Doped Zeolites and Advanced Oxidation Processes for Degradation of Azo Dyes: A Review. *Curr. Anal. Chem.* **2021**, *17*, 82–97.
20. Yang, C.X.; Dong, W.P.; Cui, G.W.; Zhao, Y.Q.; Shi, X.F.; Xia, X.Y.; Tang, B.; Wang, W.L. Highly Efficient Photocatalytic Degradation of Methylene Blue by P2ABSA-Modified TiO₂ Nanocomposite Due to the Photosensitization Synergetic Effect of TiO₂ and P2ABSA. *RSC Adv.* **2017**, *7*, 23699–23708.
21. Amaterz, E.; Tara, A.; Bouddouch, A.; Taoufyq, A.; Bakiz, B.; Benhachemi, A.; Jbara, O. Photo-Electrochemical Degradation of Wastewaters Containing Organics Catalysed by Phosphate-Based Materials: A Review. *Rev. Environ. Sci. Bio. Tech.* **2020**, *19*, 843–872.
22. Naciri, Y.; Hsini, A.; Ajmal, Z.; Navio, J.A.; Bakiz, B.; Albourine, A.; Ezahri, M.; Benhachemi, A. Recent Progress on the Enhancement of Photocatalytic Properties of BiPO₄ Using Pi-Conjugated Materials. *Adv. Colloid Interf. Sci.* **2020**, *280*, 102160.
23. Cheng, L.W.; Tsai, J.C.; Huang, T.Y.; Huang, C.W.; Unnikrishnan, B.; Lin, Y.W. Controlled Synthesis, Characterization and Photocatalytic Activity of BiPO₄ Nanostructures with Different Morphologies. *Mater. Res. Express* **2014**, *1*, 025023.
24. Lv, T.; Pan, L.K.; Liu, X.J.; Sun, Z. Enhanced Visible-Light Photocatalytic Degradation of Methyl Orange by BiPO₄-CdS Composites Synthesized Using a Microwave-Assisted Method. *RSC Adv.* **2012**, *2*, 12706–12709.
25. Shao, M.; Wang, A.W.; Cui, H.J.; Zhang, Y.Z.; Liu, Z.Y.; Xu, Y.H.; Li, Z.Y.; Xu, S. Construction of BiPO₄/CdS Heterojunction Photocatalysts for Enhanced Degradation of Organic Pollutants under Visible Light. *J. Mater. Sci. Mater. El.* **2020**, *31*, 12056–12065.
26. Zhao, X.H.; Wang, X.H.; Sun, Z.; Li, Z.Y.; Sun, D.Z. Efficient Visible-Light Photocatalytic Performance of CdS/BiPO₄ Nanoparticles Fabricated by Solvothermal Method. *Optik* **2020**, *208*, 164543.
27. Soltani, N.; Saion, E.; Yunus, W.M.M.; Navasery, M.; Bahmanrokh, G.; Erfani, M.; Zare, M.R.; Gharibshahi, E. Photocatalytic Degradation of Methylene Blue under Visible Light Using PVP-Capped ZnS and CdS Nanoparticles. *Sol. Energy* **2013**, *97*, 147–154.
28. Madkour, M.; Salih, T.; Al-Sagheer, F.; Bumajdad, A. Nano-Heterostructured Photo-Stable Cd_xZn_{1-x}S Heterojunction as a Non-Photocorrosive Visible Light Active Photocatalyst. *Opt. Mater. Express* **2016**, *6*, 002857.
29. Soltani, N.; Saion, E.; Yunus, W.M.M.; Erfani, M.; Navasery, M.; Bahmanrokh, G.; Rezaee, K. Enhancement of Visible Light Photocatalytic Activity of ZnS and CdS Nanoparticles Based on Organic and Inorganic Coating. *Appl. Surf. Sci.* **2014**, *290*, 440–447.
30. Dai, Y.D.; Lyu, R.J.; Wu, T.; Huang, C.C.; Lin, Y.W. Influences of Silver Halides AgX (X = Cl, Br, and I) on Magnesium Bismuth Oxide Photocatalyst in Methylene Blue Degradation under Visible Light Irradiation. *J. Photoch. Photobio. A Chem.* **2020**, *397*, 112585.
31. Huang, C.K.; Wu, T.; Huang, C.W.; Lai, C.Y.; Wu, M.Y.; Lin, Y.W. Enhanced Photocatalytic Performance of BiVO₄ in Aqueous AgNO₃ Solution under Visible Light Irradiation. *Appl. Surf. Sci.* **2017**, *399*, 10–19.
32. Huang, C.W.; Wu, M.Y.; Lin, Y.W. Solvothermal Synthesis of Ag Hybrid BiPO₄ Heterostructures with Enhanced Photodegradation Activity and Stability. *J. Colloid. Interf. Sci.* **2017**, *490*, 217–225.
33. Huang, T.Y.; Chen, Y.J.; Lai, C.Y.; Lin, Y.W. Synthesis, Characterization, Enhanced Sunlight Photocatalytic Properties, and Stability of Ag/Ag₃PO₄ Nanostructure-Sensitized BiPO₄. *RSC Adv.* **2015**, *5*, 43854–43862.
34. Wang, C.Y.; Wu, T.H.; Lin, Y.W. Preparation and Characterization of Bismuth Oxychloride/Reduced Graphene Oxide for Photocatalytic Degradation of Rhodamine B under White-Light Light-Emitting-Diode and Sunlight Irradiation. *J. Photoch. Photobio. A Chem.* **2019**, *371*, 355–364.
35. Deng, Y.C.; Liu, J.; Huang, Y.B.; Ma, M.M.; Liu, K.; Dou, X.M.; Wang, Z.J.; Qu, S.C.; Wang, Z.G. Engineering the Photocatalytic Behaviors of G/C₃N₄-Based Metal-Free Materials for Degradation of a Representative Antibiotic. *Adv. Funct. Mater.* **2020**, *30*, 20202002353.
36. Huang, W.G.; Wang, X.Z.; Zhang, W.T.; Zhang, S.J.; Tian, Y.X.; Chen, Z.H.; Fang, W.H.; Ma, J. Intraligand Charge Transfer Boosts Visible-Light-Driven Generation of Singlet Oxygen by Metal-Organic Frameworks. *Appl. Catal. B Environ.* **2020**, *273*, 119087.

-
37. Huang, X.X.; Zhu, N.W.; Mao, F.L.; Ding, Y.; Zhang, S.H.; Li, F.; Liu, H.R.; Wu, P.X. Novel Au@C Modified G-C₃N₄ (Au@C/G-C₃N₄) as Efficient Visible-Light Photocatalyst for Toxic Organic Pollutant Degradation: Synthesis, Performance and Mechanism Insight. *Sep. Purif. Technol.* **2020**, *252*, 117485.
 38. Chen, Y.J.; Tseng, C.S.; Tseng, P.J.; Huang, C.W.; Wu, T.H.; Lin, Y.W. Synthesis and Characterization of Ag/Ag₃PO₄ Nanomaterial Modified BiPO₄ Photocatalyst by Sonochemical Method and Its Photocatalytic Application. *J. Mater. Sci. Mater. El.* **2017**, *28*, 11886–11899.